

Provided for non-commercial research and education use.
Not for reproduction, distribution or commercial use.

		Volume 71, Number 16 August 15, 2007			
Geochimica et Cosmochimica Acta					
JOURNAL OF THE GEOCHEMICAL SOCIETY AND THE METEORITICAL SOCIETY					
Executive Editor: FRANK A. PUDDICK		Editorial Manager: LINDA TOWER Editorial Assistants: KAREN PULLIAM KERRY STEVENS			
Webmaster: ROBERT H. NICHOLLS, JR. Production Manager: CHRIS ACCER					
ADVISORS:	ROBERT C. ALLER JEFFREY C. ALT YVES ANSELIN CAROL ANASTASI MICHAEL ERIC MATTHEWS LINDA C. BURNING JAY A. BRADY ALAN D. BRADY DAVID J. BRIDGER ROBERT C. BURGESS ROBERT H. BYRNE WILLIAM H. CARRY TIMOTHY CHAPMAN ANDRÉ COMANS DAVID R. COLE LINDA J. CRESSY	JOHN CHERRY CHRISTOPHER DAVENNEY Z. H. DING CAROL M. FROST JAMES FROGGING FREDERICK A. FINE MARTIN P. GEDENSMAN JORGENSEN R. HALL T. MARK HARRISON H. ROGER HAVERTY GEORGE R. HELZ GEOFFREY F. HODGE JAMES HUNTER JIN-KIHOI HURUBE KAREN KALANICKSON CLARK JORGENSEN	NORSKO KYVA CHRISTOPH KÖRBER RICHIE KOPPEL STEPHEN M. KRÄBER S. KUROKAWA ALEXANDER N. KROT JOHN KUNZE CHRISTOPH A. LAGAN THOMAS J. LARSON MICHAEL L. MCGHEE BERNARD MERTZ JAMES MULLISON ANDRÉS MULLISON MORTEN A. MØRE JACK J. MURPHY	DAVID W. METCALLE ALFONSO MIOGGI RICHIE MILES HARUO NAGAHARA MAGNUS NORD PATRYCJA A. ODDY ERIC H. OELBERS SANDRA POZZORULLO MARK REAGAN W. IAN RICHARDS EDWARD M. RIPLEY J. KELLY RUSSELL SARA S. RUSSELL JAMES R. RUSTAD F. J. RYBICKI JÜRGEN SCHMIDT	JÜRGEN SEWALD THOMAS J. SHAW J. S. SHOOTER DAVENNY DONALD L. SOMERS GABRIEL SODRO DANIEL A. SYRIMSKY MICHAEL J. TAYLOR PETER ULLMANN DAVID J. VAUGHAN RICARDO J. WALKER LESLIE A. WARREN DAVID J. WALKOWSKI KARIN WILKE ROY A. WOODRILL CHRIS ZHU
Volume 71, Number 16		August 15, 2007			
Articles					
D. T. JOHNSON, J. FARQUHAR, D. E. CASHFIELD: Sulfur isotope insights into microbial sulfate reduction: <i>When microbes meet models</i>	3929				
T. B. COPLEN: Calibration of the calcite-water oxygen-isotope geothermometer at Devils Hole, Nevada, a natural laboratory	3948				
R. F. CARBONARO, D. M. DI TORO: Linear free energy relationships for metal-ligand complexation: Monodentate binding to negatively-charged oxygen donor atoms	3958				
W. LIU, I.-M. CHOU, R. C. BURRIGSS, Y. SONG: A unified equation for calculating methane vapor pressures in the CH ₄ -H ₂ O system with measured Raman shifts	3969				
N. G. SIMS, C. L. DE LA ROCHA, E. T. TIPPER, A. TIRPATI, A. GALEY, M. J. BICKLE: Interpreting the Ca isotope record of marine biogenic carbonates	3979				
J. HAN, H. CHEN, W. S. FYFE, Z. GAO, D. WANG, T. S. LIU: Spatial and temporal patterns of grain size and chemical weathering of the Chinese Red Clay Formation and implications for East Asian monsoon evolution	3990				
D. M. NELSON, F. S. HU, J. A. MURKEL, J. TAN, A. PEARSON: Carbon-isotope analysis of individual pollen grains from C ₃ and C ₄ grasses using a spooling-wire microcombustion interface	4005				
K. A. FARLEY: He diffusion systematics in minerals: Evidence from synthetic monazite and zircon structure phosphates	4015				
B. E. ROSENBERG, P. K. SWART, A. EBENHAUER: Constraining initial ²³⁰ Th activity in incrementally deposited, biogenic aragonite from the Bahamas	4025				
E. GARDIEN, J.-M. MONTEIL, A.-M. SEYDOUX-GUILLEME, R. WICHT: Pb diffusion in monazite: New constraints from the experimental study of Pb ²⁺ and Ca ²⁺ interdiffusion	4036				
D. TRAIL, S. J. MOZZES, T. M. HARRISON: Thermal events documented in Hadean zircons by ion microprobe depth profiles	4044				
N. M. MILLS, C. B. AZEL, D. S. DRAPER: Metal-silicate partitioning of cesium: Implications for core formation	4066				
<i>Continued on outside back cover</i>					

This article was published in an Elsevier journal. The attached copy is furnished to the author for non-commercial research and education use, including for instruction at the author's institution, sharing with colleagues and providing to institution administration.

Other uses, including reproduction and distribution, or selling or licensing copies, or posting to personal, institutional or third party websites are prohibited.

In most cases authors are permitted to post their version of the article (e.g. in Word or Tex form) to their personal website or institutional repository. Authors requiring further information regarding Elsevier's archiving and manuscript policies are encouraged to visit:

<http://www.elsevier.com/copyright>



Metal-silicate partitioning of cesium: Implications for core formation

Nathan M. Mills, Carl B. Agee^{*}, David S. Draper

Institute of Meteoritics, University of New Mexico, Albuquerque NM 87131-1126, USA

Received 14 November 2006; accepted in revised form 24 May 2007; available online 13 June 2007

Abstract

Here we present the first set of metal-silicate partitioning data for Cs, which we use to examine whether the primitive mantle depletion of Cs can be attributed to core segregation. Our experiments independently varied pressure from 5 to 15 GPa, temperature from 1900 to 2400 °C, metallic sulfur content from pure Fe to pure FeS, silicate melt polymerization, expressed as a ratio of non-bridging oxygens to tetrahedrally coordinated cations (nbo/t) from 1.26 to 3.1, and fO_2 from two to four log units below the iron-wüstite buffer. The most important controls on the partitioning behavior of alkalis were the metallic sulfur content, expressed as X_S , and the nbo/t of the silicate liquid. Normalization of X_S to 0.5 yielded the following expressions for D -values as a function of nbo/t: $\log D_{Na} = -2.0 + 0.44 \times (\text{nbo}/t)$, $\log D_K = -2.4 + 0.67 \times (\text{nbo}/t)$, and $\log D_{Cs} = -3.2 + 1.17 \times (\text{nbo}/t)$. Normalization of nbo/t to 2.7 resulted in the following equations for D -values as a function of S content: $\log D_{Na} = -4.1 + 6.4 \times X_S$, $\log D_K = -7.7 + 13.9 \times X_S$, and $\log D_{Cs} = -12.1 + 23.3 \times X_S$.

There appears to be a negative pressure effect up to 15 GPa, but it should be noted that this trend was not present before normalization, and is based on only two measurements. There is a positive trend in cesium's metal-silicate partition coefficient with increasing temperature. D_{Cs} exhibits the largest change and increased by a factor of three over 500 °C. The effect of oxygen fugacity has not been precisely determined but in general, lowering fO_2 by two log units resulted in a rise in all D -values of approximately an order of magnitude. In general, the sensitivity of partition coefficients to changing parameters increased with atomic number.

The highest D -value for Cs observed in this study is 0.345, which was obtained at nbo/t of 2.7 and a metal phase of pure FeS. This metallic composition has far more S than has been suggested for any credible core-forming metal. We therefore conclude that the depletion of Cs in Earth's mantle is either caused by radically different behavior of Cs at pressures higher than 15 GPa or is not related to core formation. Even so, we have shown that a planet with a sufficient S inventory may incorporate significant amounts of alkali elements into its core.

© 2007 Elsevier Ltd. All rights reserved.

1. INTRODUCTION

The difficulty in explaining the elemental abundance pattern of the mantle has led some scientists to conclude that the Earth accreted heterogeneously, and without melting, from a combination of previously differentiated materials (e.g., Wänke, 1981). This approach is somewhat unsatisfying, because any new revelations regarding mantle or core

composition can be explained by slightly altering the composition or order of the heterogeneous components. Fortunately, recent advances in high-pressure experimental petrology, such as multi-anvil (e.g., Agee et al., 1995) and diamond-anvil experiments (e.g., Bouhifd and Jephcoat, 2003), have allowed us to develop viable homogeneous accretion models (e.g., Li and Agee, 1996; Richter et al., 1997) as alternatives to heterogeneous scenarios.

If the Earth experienced a widespread melting event after accretion, the stage would have been set for equilibrium differentiation of the core. Under those conditions, it may be possible to constrain equilibrium conditions of core

^{*} Corresponding author.

E-mail address: agee@unm.edu (C.B. Agee).

segregation by relating an element's estimated abundance in the primitive mantle (i.e., prior to crust extraction) to its presumed abundance in the bulk Earth. The difference between those abundances could be attributed to the partitioning of the element into a descending metal phase with the same major element composition as the core (McDonough, 2004). A given element will partition into the metal phase to a degree determined by its metal-silicate partition coefficient, which, for an element i , is given by $D_i = C_i^{\text{metal}}/C_i^{\text{silicate}}$, where C_i is the concentration of i in the given phase and D_i is the partition coefficient of i between metal and silicate. Thus, if the homogeneous-accretion/equilibrium differentiation model is correct, we should be able to explain the inferred observed mantle elemental abundances by calculating an appropriate D_i for each element. A coherent set of conditions that generate the correct D -values for all elements would constrain the parameters of the magma ocean from which the core segregated (Righter, 2003).

Because there are several parameters that may influence the partitioning of a given element, including pressure, temperature, metal and silicate composition, and oxygen fugacity, there is a large body of work in print that studies some combination of these parameters (e.g., Jones and Walker, 1991; Li and Agee, 1996; Gessmann and Rubie, 1998; Jaeger and Drake, 2000; Bouhifd and Jephcoat, 2003). Many use the planetary volatility trend (Fig. 1) as a starting point for abundances, which describes the abundance of an element relative to CI chondrites and refractory elements based on its solar nebula condensation temperature (McDonough and Sun, 1995; Palme and O'Neill, 2004). Most of these studies emphasized the effect of one or two parameters that affect the element in question. In spite of the fact that most of these studies have determined strong correlations between partitioning behavior and the parameters studied, no consistent set of conditions for a magma ocean has evolved (Chabot et al., 2005; Wade and Wood, 2005). That may be in part because the partitioning experiments designed to address this question so far have focused on siderophile elements, which by definition preferentially partition into the metal phase and were likely removed from the mantle during core formation, and therefore do not lie on the volatility trend. D -values for these elements are always >1 , and for the Highly Siderophile Elements (HSEs), can be on the order of 10^6 – 10^{12} . Most importantly, because these elements are always siderophile, there may be a broad range of conditions under which they would be depleted to the degree necessary to explain their deviation from expected mantle abundance.

This study attempts to determine whether and to what degree Cs, a lithophile element that does not fall on the volatility trend, may become siderophile under conditions applicable to core formation. Normally, a lithophile element would not be useful for understanding conditions of core formation, but it may be possible to account for the depletion of Cs via a very specific set of conditions during core formation under which Cs became siderophile. Some partition experiments have been done on the alkali elements under high-pressure conditions, usually in relation to the possibility of incorporating K into the core as a heat source

(e.g., Gessmann and Wood, 2002; Murthy et al., 2003) but no data at all are available on the metal-silicate partitioning behavior of Cs. We have used high-pressure and high-temperature experiments to determine whether Cs becomes siderophile under realistic core-formation conditions. In the following sections, we present our procedures, results, and analysis of the partitioning behavior of Cs.

2. EXPERIMENTAL PROCEDURES

2.1. Starting materials

The silicate portions of most starting compositions for this study were prepared from a mixture of oxide powders. These mixtures approximated a primitive mantle composition with respect to major element ratios (Al, Fe, Mg, and Ca) with the exception of SiO_2 , which was varied to adjust the basicity of the silicate melt. Because there are few stable compounds of Cs, the base mixture was doped with pollucite, a $\text{Cs}_2\text{Al}_2\text{Si}_4\text{O}_{12}\cdot 2\text{H}_2\text{O}$ zeolite mineral, which was kindly provided by the American Museum of Natural History. In addition, carbonates of Na and K were added to the mixture in order to allow comparison to other partitioning experiments. All alkalis were doped to approximately 3% by weight to avoid possible Henry's Law violations. Each mixture was loaded into a Pt crucible, dehydrated and decarbonated at 1000 °C for one hour in a gas-mixing Deltech furnace at 1 bar. During dehydration/decarbonation, the H_2/CO_2 mix was held at approximately the iron-wüstite (IW) oxygen buffer to prevent excessive oxidation of the starting material.

The metallic portion of the starting composition was a combination of iron powder, iron sulfide, sulfur, and iron silicide, depending on the desired S content and oxygen fugacity of the experiment. Metals were added to the decarbonated silicate to approximately 30% of the final weight. This relatively large amount of metal ensured that final run products would have metal blobs large enough to easily identify and analyze without silicate contamination. Nickel was not added to any of the starting compositions because the absence of 10 wt% nickel is not likely to significantly affect the measured partition coefficients (Righter and Drake, 2000).

Runs A275 and A276 were part of an exploratory set of experiments and were pure pollucite mixed with FeS. These compositions, along with those described previously, are listed in Table 1.

2.2. Run conditions

Sample starting materials were loaded into graphite capsules and encased in Ceramacast[®] 584 octahedra. Runs were generally not conducted in MgO or alumina capsules because they reacted with the sample and altered the chemistry of the final run product to an unpredictable degree. Metallic capsules were not used because they alloyed with the molten Fe in the charge, melted, and destroyed the heater. The octahedra were fitted with a cylindrical Re heater and a $\text{W}_3\text{Re}/\text{W}_{25}\text{Re}$ thermocouple. Following assembly, the octahedra were mounted onto tungsten carbide cubes,

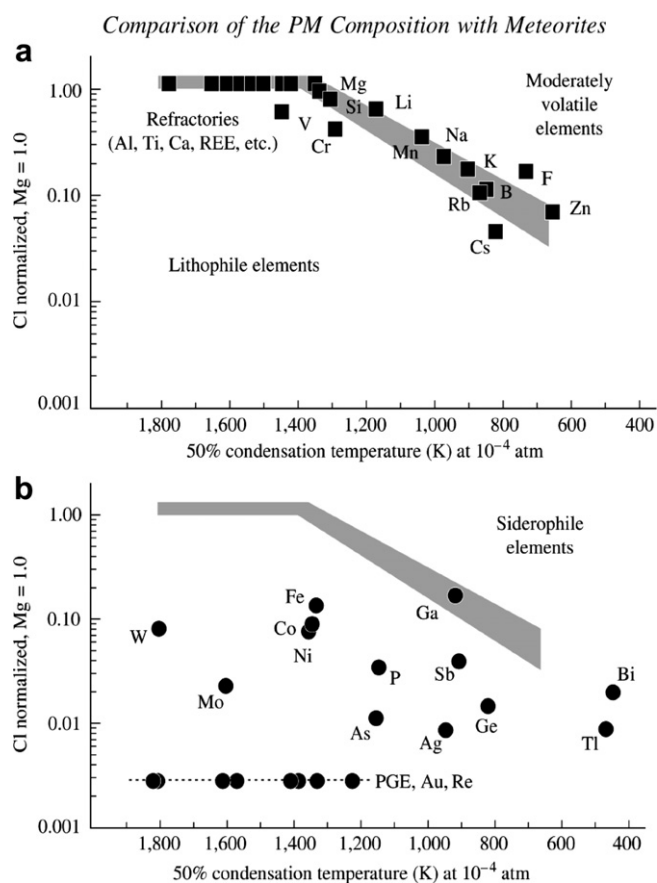


Fig. 1. Inferred abundances of (a) lithophile and (b) siderophile elements in the primitive mantle (i.e., prior to crust extraction) relative to CI chondrites and refractory elements (Palme and O'Neill, 2004; originally from McDonough and Sun, 1995). The difference between observation (black circles) and the expected abundance from the volatility trend (shaded gray) is attributed to core subtraction.

with truncated edge lengths (TEL) of 8 mm for experiments <10 GPa and 6 mm for experiments up to 15 GPa. The appropriate pressure was applied by a Walker-style multi-anvil press, located at the University of New Mexico's High-Pressure Experimental Petrology laboratory, calibrated by performing transformations of quartz to coesite (~3 GPa), coesite to stishovite (~9.5 GPa), and olivine to spinel (~14 GPa). A complete treatment of the Walker multi-anvil method is presented by Agee et al. (1995).

Experiments were generally held at target conditions for 2 min, which has been shown by time-series experiments to be more than adequate to attain equilibrium in completely molten charges at high temperature and pressure (e.g., Gessmann and Rubie, 1998). Some experiments ended before the planned stop time due to the consumption and destruction of the Re heater. In these cases, equilibrium was verified by the absence of chemical zoning in either the metallic or silicate portions of the quenched run product. Quenching was normally obtained by cutting power to the heater, and the initial quench rate obtained was approximately 500 °C/s. No charges exhibited any sign of equilibrium crystal growth, although many did show either a mottled or a spinifex silicate texture, which evolved during the quenching process.

After removal from the multi-anvil assembly, the run products were extracted and mounted in epoxy. Alkali ele-

ments in a sulfide phase are known to be soluble in water (Chabot and Drake, 1999), so all contact with liquids was avoided. Initial grinding was done on a dry diamond disc until the sample was exposed. The samples were not re-impregnated with epoxy to fill the decompression cracks to avoid possible leaching of alkalis from the metal phase. Polishing was done on a series of carbide sheets without lubricant, then finished to a 1 micron polish on lapping papers, following the technique of Murthy et al. (2003). The high-pressure run products were polished to 6 microns exclusively on diamond discs because the capsules, which turned to diamond above 6 GPa, could not be ground or polished with carbide sheets or lapping papers. Between grades of polishing, the decompression cracks were cleared of debris with an air duster. The lack of water in the process forced polishing to be performed with as few strokes as possible to avoid pieces of the sample breaking off and gouging the face of the sample as they were excavated. Typically, samples had large scratches across the finished surface, but this was not found to interfere with analysis, as long as there were sufficient areas of fine polish. Due to the extremely high reactivity of alkali metals with water, care was taken not to leave the samples exposed to air. All samples were polished as soon as practical before analysis, carbon coated immediately, and stored in an evacuated desiccation chamber until analysis. Failure to follow this

Table 1
Experimental run conditions and alkali partition coefficients

Run #	<i>P</i> (GPa)	<i>T</i> (K)	Silicate	Metal	nbo/ <i>t</i>	ΔIW	X_S	D_{Cs}	D_K	D_{Na}
A275	3.5	2148	Pollucite	FeS	0.04	-2.6	0.51	0.018 (0.004)	n.m.	n.m.
A275	3.5	2148	Pollucite	FeS	0.04	-2.6	0.52	0.016 (0.001)	0.084 (0.015)	0.041 (0.017)
A276	3.5	2148	Pollucite	FeS	0.04	-2.7	0.51	0.019 (0.002)	n.m.	n.m.
A276	3.5	2148	Pollucite	FeS	0.09	-2.7	0.53	0.015 (0.004)	n.m.	n.m.
A332	5	2373	v1.1	FeS	1.26	-1.9	0.51	0.033 (0.007)	0.038 (0.006)	0.024 (0.004)
A351	5	2373	v1.8	FeS	1.93	-1.8	0.49	0.055 (0.013)	0.070 (0.034)	0.069 (0.043)
A325	5	2373	v2.5	FeS	2.30	-2.2	0.48	0.109 (0.028)	0.067 (0.015)	0.059 (0.013)
A333	5	2373	v2.7	FeS	2.74	-2.2	0.45	0.345 (0.135)	0.119 (0.056)	0.175 (0.058)
A326	5	2373	v3.0	FeS	3.08	-2.3	0.46	0.201 (0.089)	0.141 (0.031)	0.095 (0.041)
A340	5	2373	v3.0	FeS	2.99	-2.3	0.47	0.180 (0.054)	0.074 (0.026)	0.043 (0.020)
A336 ^{a,b,c}	5	2373	v2.7	Fe	2.94	-2.4	0.00	0.008 (0.005)	0.001 (0.004)	0.000 (0.001)
A339 ^c	5	2373	v2.7	Fe, FeS	2.97	-2.1	0.21	0.011 (0.007)	0.012 (0.015)	0.005 (0.005)
A354 ^c	5	2373	v2.7	Fe, FeS	3.78	-1.9	0.34	0.010 (0.003)	0.004 (0.005)	0.008 (0.004)
A355 ^{a,b}	5	2373	v2.7	Fe, FeS	3.26	-1.9	0.33	0.009 (0.008)	0.012 (0.011)	0.009 (0.009)
A338	5	2373	v2.7	Fe, FeS	3.10	-1.9	0.41	0.028 (0.008)	0.066 (0.029)	0.037 (0.014)
A346	5	2173	v2.5	FeS	2.49	-2.1	0.48	0.100 (0.032)	0.060 (0.012)	0.062 (0.022)
A342	5	2373	v2.5	FeS	2.43	-2.2	0.47	0.112 (0.025)	0.083 (0.020)	0.098 (0.024)
A343	5	2673	v2.5	FeS	2.18	-2.2	0.48	0.137 (0.023)	0.064 (0.011)	0.081 (0.021)
A344	5	2673	v2.5	FeS	2.25	-2.1	0.47	0.127 (0.012)	0.084 (0.010)	0.079 (0.014)
A360 ^{a,b,c}	5	2373	v2.5	FeS, FeSi, S	2.42	-4.6	0.23	0.009 (0.008)	0.016 (0.019)	0.005 (0.005)
A357	5	2373	v2.5	FeS, FeSi, S	2.72	-4.2	0.34	0.014 (0.009)	0.007 (0.008)	0.004 (0.003)
A356	5	2373	v2.5	FeS, FeSi, S	2.63	-4.0	0.40	0.057 (0.045)	0.601 (0.399)	0.089 (0.052)
A363 ^c	5	2373	v2.5	FeS, FeSi, S	1.96	-4.2	0.43	0.030 (0.011)	0.039 (0.062)	0.048 (0.058)
A372	5	2673	v2.7	FeS	1.82	-2.2	0.44	0.215 (0.061)	0.232 (0.141)	0.218 (0.147)
A369	15	2673	v2.7	FeS	2.64	-2.4	0.46	0.224 (0.204)	0.245 (0.300)	0.177 (0.161)

Errors in parentheses are $\pm 1\sigma$.

n.m = not measured.

With the exception of runs A275 and A276, all silicate compositions are mixtures of simple oxides. The number preceded by the letter "v" is the intended nbo/*t* of the silicate.

^a Cs analyses below detection limits.

^b K analyses below detection limits.

^c Na analyses below detection limits.

practice rendered several charges useless due to reaction of the alkali metals with moisture in the air and eventual rusting of the metal phase.

2.3. Analytical technique

All run products were analyzed on a JEOL 8200 electron microprobe operating at a 15 kV accelerating potential and using a 20 nA beam current. Commercially available Cs₂MoO₄ was analyzed by XRD to verify its purity and compressed into a small disc. This disc was used as a standard, with elemental abundances assigned based on stoichiometry, to analyze a piece of natural pollucite. Because the pollucite crystal was more durable than the compressed powder disc, the results of this analysis were entered as a reference composition and the pollucite crystal was used as the Cs standard for all further analyses. Tests for possible Cs volatility in the pollucite under the electron beam were performed under a variety conditions (15 kV, 20 nA, 0, 10 and 20 micron spot size, 15 kV, 10 nA, 0, 10, and 20 micron spot size) for 120 s counting times. Under all conditions counts/second remained remarkably stable indicating that Cs-loss is not an issue for these analyses.

A series of analyses was done to examine the effect of sample heating on retention of alkalis in the sample, with

the results presented in Section 3.1. Major and minor elements were counted for 20–30 s, and the trace elements of interest (Cs, K, and Na) were counted for 40 s. L-alpha X-ray lines were used for Cs, and K-alpha for Na and K. The alkali elements were always counted first on their assigned spectrometer to avoid heat-related loss.

Except for the least mafic compositions, the silicate exhibited a heterogeneous quench texture, with alkali-rich and -poor zones up to 10 m wide. In addition, the metal phase was commonly heterogeneous, especially in the experiments combining iron silicide with FeS, which create immiscible liquids at our run conditions. The textures in the run products required the use of a defocused beam of 20 μ m to obtain representative averaged compositions of each phase.

Carbon content of the metal phase was not explicitly measured. In general, the totals for analyses of the metal phase were \sim 95%. As with other experiments in graphite capsules (e.g., Chabot and Agee, 2003), some C was expected to dissolve into the metal phase during the run. However, experiments run in MgO or alumina capsules also had low metallic totals, therefore the deviation from 100% is more likely attributed to the rough surface of the metal phase. Oxygen was explicitly measured in the metal, using hematite as a standard, and was generally less than 2%.

The oxygen did not exsolve into oxygen-rich blobs within the metal phase, as has complicated analysis in other studies (e.g., Chabot and Agee, 2003). Aluminum and calcium were analyzed in the metal phase as a check for silicate contamination.

2.4. Calculation of run parameters

Oxygen fugacity (fO_2) was calculated relative to the IW buffer (ΔIW) by the relation $\Delta IW = 2 \log (a_{Fe}/a_{FeO})$, where a_{Fe} and a_{FeO} are the activities of Fe in the metal phase and that of FeO in the silicate. The activity coefficients for both Fe and FeO were assumed to be unity, so the reported oxygen fugacities are based on mole fractions of Fe and FeO (X_{Fe} and X_{FeO} , respectively) in their host phase. This approximation is probably least accurate for the metal phase, where X_{Fe} is as low as 0.5, but even an activity coefficient of 0.5 changes the estimate of oxygen fugacity by only 0.6 log units. This is acceptable for this study, because the goal is not to parameterize the effect of oxygen fugacity on partitioning, but to sense the effect of relative change. For simplicity we selected an activity coefficient of 1 for the silicate phase.

The degree of polymerization in the silicate melt was expressed using the parameter nbo/t , which describes the ratio of non-bridging oxygens (nbo) present in a melt to the number of tetrahedrally coordinated cations (t) (Mysen and Virgo, 1980). Following the general guidance of Mysen (1983), the ratio was calculated as $nbo/t = Z_{nbo}/Z_t$, where Z_{nbo} and Z_t are the molar concentrations of non-bridging oxygens and tetrahedrally coordinated cations, respectively. Further, $Z_{nbo} = 2*[X_{Fe} + X_{Mg} + X_{Ca}] + [X_{Na} + X_K + X_{Cs} - X_{Al}]$ and $Z_t = X_{Si} + X_{Al}$. This calculation is simplified by the absence of most minor elements, the low concentrations of Al, and the assumed absence of Fe^{3+} due to the low oxygen fugacity. Completely polymerized melts, such as molten feldspar, would have $nbo/t = 0$, and completely depolymerized melts, such as molten olivine, would have $nbo/t = 4$.

Errors in the reported D -value are calculated using the following formula: $\sigma_D = D \sqrt{(\frac{\sigma_A}{A})^2 + (\frac{\sigma_B}{B})^2}$ where D is the nominal D -value, A and B are the wt% in each phase, and σ_A and σ_B are the standard deviations of measurements in each phase. Even using a defocused beam, the standard deviation in the analyses is rather large due to the range of alkali concentrations within a given phase, so errors in D -values are reported to $\pm 1\sigma$. The D -values reported in Table 1 reflect the average of at least seven analyses of each phase in the run product. Using this averaging method, analysis of identical samples at different times yielded concentrations and totals within the 1σ error (see Fig. 2).

3. RESULTS

3.1. Volatility measurements

We first demonstrated that the volatilization of Cs was not a confounding factor in our experiments. A pair of experiments was conducted to investigate the possible loss of Cs during the run, which has been reported for K (Mur-

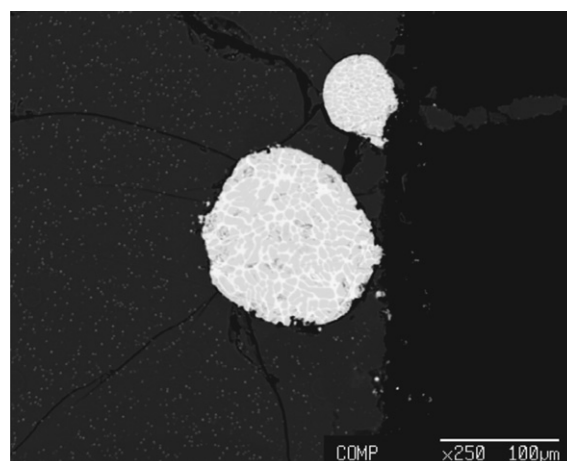


Fig. 2. Back-scattered electron image of run #A363 showing the heterogeneous texture of the metal phase. The dark portions were dominantly FeS, and the light portions had slightly less S. Alkali metal concentrations, though variable, were not correlated with the differences in local S content. This run had a fairly homogeneous silicate phase, with small ($<5 \mu m$) metal blebs spaced throughout. The dispersed metal blebs were small and widely spaced enough allowed for silicate analysis without significant contamination by metal.

thy et al., 2003). Identical compositions were run under identical conditions, with one sample in an unsealed graphite capsule (A275) and the other in a Pt-sealed graphite capsule (A276). There was no significant difference between the runs, as measured by D_{Cs} and the absolute amount of Cs retained in either phase of both charges. The data from each of those runs are listed in Tables 2 and 3.

To investigate the possibility of Cs mobilization and loss under the heat of the electron beam, we took two approaches. The first was to measure the number of counts per second (cps) at different counting times on pristine areas of sample. Peak intensities were always measured before background, and count times ranged from 10 to 60 s. Measured cps did not significantly vary in this series of analyses in either phase (Fig. 3a). Because alkali concentration in the metal commonly varies by 10% relative, the minor deviations in metal cps at 40 and 60 s can be attributed to the heterogeneity of the phase.

The second method was to immediately repeat an analysis multiple times at a stationary point on the sample. In this case, the cps are fairly constant in both phases over five analyses using a $20 \mu m$ beam for 40 s on peak and 20 s on background (Fig. 3b). This method heated the analysis point for a total of about six minutes, and the fact that cps were unchanging over this period means that the metal cps variation of Fig. 3a was definitely not due to sample heating. In fact, sample heating was an issue only when the beam diameter was reduced to the minimum possible ($1 \mu m$ nominal) on the silicate phase. Under those conditions, there was significant loss of Cs in each successive analysis. This loss was not observed with a small-diameter beam in the metal phase, and is not plotted in Fig. 3b. We therefore conclude that the use of a broad beam to average out sample heterogeneities in our analyses minimized Cs loss due to heating.

Table 2
Metallic liquid compositions

Run#	Si	Fe	S	Cs	K	Na	O	Total
A275	0.01 (0.01)	59.92 (0.36)	36.74 (0.66)	0.46 (0.10)	n.m.	n.m.	n.m.	97.13
A275	0.01 (0.01)	59.05 (0.60)	37.16 (0.41)	0.40 (0.04)	0.04 (0.01)	0.05 (0.02)	n.m.	96.71
A276	0.02 (0.02)	58.75 (0.36)	36.38 (0.67)	0.48 (0.05)	n.m.	n.m.	n.m.	95.62
A276	0.06 (0.11)	58.7 (1.5)	38.9 (1.1)	0.39 (0.10)	n.m.	n.m.	n.m.	98.14
A332	0.09 (0.06)	56.72 (0.47)	36.88 (0.44)	0.09 (0.02)	0.07 (0.01)	0.11 (0.02)	0.98 (0.15)	94.94
A351	0.03 (0.02)	59.46 (0.56)	35.96 (0.71)	0.17 (0.03)	0.19 (0.11)	0.24 (0.11)	1.34 (0.41)	97.39
A325	0.01 (0.00)	60.98 (0.34)	34.80 (0.25)	0.28 (0.04)	0.20 (0.03)	0.22 (0.05)	1.00 (0.20)	97.48
A333	0.10 (0.05)	58.6 (1.3)	33.23 (0.57)	1.05 (0.40)	0.42 (0.14)	0.48 (0.22)	2.71 (0.93)	96.56
A326	0.01 (0.01)	61.26 (0.55)	33.63 (0.27)	0.32 (0.12)	0.24 (0.09)	0.50 (0.08)	1.75 (0.21)	97.71
A340	0.02 (0.03)	60.45 (0.70)	34.04 (0.21)	0.25 (0.04)	0.08 (0.04)	0.16 (0.04)	1.29 (0.20)	96.29
A336	0.01 (0.01)	91.97 (0.45)	0.02 (0.00)	0.02 (0.01)	0.00 (0.00)	0.00 (0.01)	0.14 (0.02)	92.17
A339	0.01 (0.01)	81.4 (7.7)	12.5 (9.2)	0.04 (0.02)	0.01 (0.01)	0.04 (0.05)	0.29 (0.15)	94.30
A354	0.01 (0.01)	71.65 (0.97)	21.5 (1.0)	0.03 (0.01)	0.02 (0.01)	0.02 (0.02)	0.51 (0.08)	93.78
A355	0.00 (0.00)	74.5 (1.2)	22.2(1.2)	0.03 (0.03)	0.02 (0.02)	0.05 (0.04)	1.5(1.0)	98.31
A338	0.01 (0.01)	65.5 (1.7)	28.6 (1.6)	0.08 (0.02)	0.09 (0.03)	0.21 (0.09)	1.74 (0.33)	96.17
A346	0.02 (0.01)	61.64 (0.42)	35.04 (0.39)	0.28 (0.07)	0.20 (0.06)	0.15 (0.03)	1.28 (0.21)	98.62
A342	0.07 (0.05)	60.78 (0.85)	34.93 (0.47)	0.28 (0.04)	0.30 (0.05)	0.26 (0.06)	1.86 (0.35)	98.47
A343	0.01 (0.01)	61.65 (0.38)	35.40 (0.18)	0.35 (0.05)	0.25 (0.06)	0.20 (0.03)	1.30 (0.14)	99.16
A344	0.05 (0.02)	60.95 (0.78)	34.67 (0.30)	0.35 (0.03)	0.25 (0.04)	0.26 (0.03)	1.65 (0.10)	98.17
A360	8.1 (7.1)	74.0 (9.2)	15.4 (14.8)	0.02 (0.01)	0.01 (0.01)	0.04 (0.04)	0.25 (0.28)	97.78
A357	0.95 (0.35)	71.9 (2.7)	22.0 (2.8)	0.04 (0.02)	0.01 (0.01)	0.02 (0.02)	0.20 (0.07)	95.07
A356	0.13 (0.13)	61.7 (1.1)	28.8 (1.2)	0.10 (0.08)	0.15 (0.07)	1.13 (0.64)	2.3 (1.0)	94.38
A363	0.01 (0.01)	69.7 (1.2)	30.8 (1.3)	0.08 (0.03)	0.15 (0.18)	0.12 (0.18)	0.52 (0.69)	101.32
A372	0.02 (0.01)	60.52 (0.97)	34.48 (0.66)	0.57 (0.16)	0.47 (0.31)	0.66 (0.40)	3.6 (1.4)	100.31
A369	0.09 (0.06)	63.41 (0.79)	33.9 (1.6)	0.09 (0.07)	0.06 (0.05)	0.10 (0.11)	1.45 (0.88)	99.09

n.m., not measured.

Analyses are reported in wt%. Errors in parentheses are $\pm 1\sigma$.

3.2. Pressure

The pressure range of our experiments extended from 5 to 15 GPa. The observed D -values for all alkali elements remained virtually unchanged across this pressure range. As shown in Fig. 4, the calculated errors for the 15 GPa data are extremely large. Analysis of this run product was complicated by the difficulty in dry-polishing, as the graphite capsule had converted to diamond. The sample was excavated to below the level of the diamond capsule and could not be well polished. Although the metal phase analyses were similar to those in other run products, the totals for the silicate phase were much lower, near 85%. This is most likely due to the rough surface (Fig. 5).

3.3. Temperature

A set of experiments was conducted at 5 GPa, 35 wt% S in the metal, and nbo/t of approximately 2.2. The temperature range of this set extended from 1900 to 2400 °C, which was as large as possible to maintain a completely molten sample and not exceed the maximum temperature allowed by our temperature controller. The temperature range could have been extended by approximately 100 °C by lowering the operating pressure, but it was found that experiments were much less stable at very high temperatures below 5 GPa. Although all partition coefficients for a given element were within error of one another, the absolute value of D_{Cs} did rise from 0.100 at 1900 °C to 0.137 at 2400 °C (Fig. 6). D_{Na} and D_K did not exhibit the apparent trend of D_{Cs} .

3.4. Silicate composition

A series of experiments designed to examine the effect of melt polymerization was conducted at 5 GPa, 2100 °C, and 35 wt% S in the metal. The nbo/t of the silicate melts varied from 1.2 to 2.9, and the rise in D_{Cs} was closely correlated with the rise in nbo/t . The minimum D_{Cs} of 0.03 was found at $nbo/t = 1.2$, and the maximum of 0.345 was found at $nbo/t = 2.67$. D_{Na} and D_K exhibited the same general behavior, but with weaker correlations than D_{Cs} . In addition, the D -values for Na and K were less sensitive to changes in nbo/t than for Cs. In almost all cases, D_{Cs} was greater than both D_{Na} and D_K . In general, dependence on degree of melt polymerization provides the most reliable and well-defined trend for the partitioning of all three alkalis.

3.5. Metallic composition

At otherwise constant composition and run conditions, the S content of the starting material was varied from 0% (pure Fe) to 36% (pure FeS). Partition coefficients for all alkali elements were very strongly dependent on the S content of the metal, remaining at or below detection limits at S contents below 25%. For example, of all individual point analyses on compositions with <25% S, over 60% were below detection limits for Cs, with the proportion dramatically higher for the lowest S contents. The dashed lines in Fig. 8 represent the highest D -value calculated for which four or more of the individual points were below detection limits. D -values at or below this line are judged to be

Table 3
Silicate liquid compositions

Run #	Si	Al	Fe	Mg	Ca	S	Cs	K	Na	O	Total
A275	22.6 (0.06)	8.04 (0.04)	1.5 (0.06)	0.02 (0.01)	0.04 (0.01)	0.25 (0.02)	26.73 (0.03)	0.45 (0.01)	1.21 (0.01)	35.1	95.9
A275	22.7 (0.10)	8.73 (0.04)	1.48 (0.04)	0.03 (0.01)	n.m	0.26 (0.02)	26.21 (0.03)	0.47 (0.01)	1.21 (0.01)	35.7	96.8
A276	22.5 (0.08)	8.04 (0.04)	1.3 (0.09)	0.03 (0.01)	0.05 (0.01)	0.23 (0.02)	26.36 (0.06)	0.47 (0.00)	1.22 (0.01)	37.6	97.8
A276	22.8 (0.09)	9.15 (0.02)	1.35 (0.04)	0.04 (0.01)	0.04 (0.02)	0.23 (0.02)	26.02 (0.03)	0.48 (0.01)	1.20 (0.01)	36.8	98.1
A332	26.7 (0.12)	2.24 (0.02)	4.8 (0.15)	10.9 (0.19)	1.09 (0.03)	0.47 (0.10)	2.91 (0.06)	2.83 (0.06)	2.85 (0.02)	43.9	98.7
A351	20.2 (0.37)	2.33 (0.02)	5.0 (0.37)	13.3 (0.57)	1.2 (0.07)	0.67 (0.20)	3.32 (0.23)	2.76 (0.19)	3.42 (0.15)	38.6	90.8
A325	20.5 (0.42)	2.53 (0.06)	3.8 (0.15)	18.1 (0.50)	1.7 (0.25)	0.29 (0.09)	2.73 (0.28)	3.31 (0.25)	3.23 (0.09)	41.6	97.8
A333	18.2 (0.28)	2.82 (0.06)	3.4 (0.31)	19.8 (0.28)	1.9 (0.20)	0.57 (0.16)	3.18 (0.15)	2.43 (0.10)	4.06 (0.09)	41.0	97.4
A326	18.2 (0.46)	2.18 (0.09)	3.7 (0.27)	22.2 (0.71)	1.8 (0.38)	0.54 (0.11)	1.64 (0.20)	2.50 (0.29)	3.55 (0.27)	41.8	98.1
A340	18.2 (0.45)	2.75 (0.24)	3.7 (0.25)	23.0 (1.29)	1.9 (0.46)	0.72 (0.13)	1.47 (0.19)	1.97 (0.22)	2.14 (0.23)	42.4	98.3
A336	17.9 (0.14)	2.73 (0.07)	6.1 (0.17)	20.8 (0.68)	1.9 (0.17)	0.01 (0.00)	3.26 (0.11)	2.74 (0.09)	3.40 (0.11)	41.0	99.8
A339	17.6 (0.13)	2.86 (0.08)	6.9 (0.19)	20.3 (0.70)	1.9 (0.12)	0.33 (0.03)	3.73 (0.12)	2.61 (0.09)	3.28 (0.12)	41.1	100.5
A354	13.3 (0.18)	2.81 (0.10)	7.0 (0.37)	19.9 (1.41)	1.7 (0.14)	0.39 (0.04)	3.13 (0.16)	2.63 (0.15)	4.37 (0.48)	36.3	91.5
A355	15.6 (0.27)	2.80 (0.04)	7.0 (0.22)	19.7 (0.72)	1.7 (0.13)	0.35 (0.02)	3.50 (0.06)	2.64 (0.12)	3.88 (0.29)	38.6	95.9
A338	17.5 (0.09)	2.60 (0.05)	6.4 (0.21)	21.1 (0.40)	1.7 (0.09)	0.53 (0.10)	3.03 (0.08)	2.53 (0.06)	3.22 (0.07)	41.3	100.1
A346	19.9 (0.64)	2.33 (0.12)	4.0 (0.15)	19.3 (0.47)	1.5 (0.36)	0.46 (0.07)	2.95 (0.27)	3.15 (0.33)	2.57 (0.05)	41.7	98.0
A342	20.3 (0.41)	2.68 (0.08)	3.9 (0.22)	19.5 (0.50)	1.7 (0.25)	0.40 (0.12)	2.61 (0.21)	3.03 (0.24)	3.09 (0.07)	42.6	99.8
A343	19.8 (0.20)	3.87 (0.04)	3.9 (0.23)	18.0 (0.37)	1.7 (0.12)	0.50 (0.11)	2.70 (0.10)	3.11 (0.11)	3.09 (0.07)	42.3	98.9
A344	19.9 (0.16)	3.29 (0.07)	4.1 (0.34)	17.9 (0.21)	1.7 (0.07)	0.54 (0.18)	2.86 (0.07)	3.22 (0.07)	3.06 (0.07)	42.0	98.6
A360	22.5 (0.31)	2.41 (0.01)	0.3 (0.08)	17.0 (0.07)	1.5 (0.06)	6.27 (0.07)	2.04 (0.01)	2.13 (0.01)	2.28 (0.01)	50.4	106.8
A357	18.0 (0.12)	2.58 (0.02)	0.5 (0.06)	17.2 (0.05)	1.6 (0.05)	4.15 (0.04)	2.68 (0.02)	2.78 (0.02)	2.65 (0.02)	42.8	94.9
A356	18.4 (0.11)	3.72 (0.21)	0.5 (0.11)	16.8 (0.09)	1.5 (0.08)	6.24 (0.18)	1.89 (0.03)	1.86 (0.02)	2.09 (0.02)	46.6	99.6
A363	23.9 (0.08)	2.64 (0.02)	0.5 (0.10)	17.9 (0.13)	1.7 (0.04)	1.67 (0.11)	2.73 (0.02)	3.05 (0.01)	2.96 (0.01)	46.5	103.5
A372	17.1 (0.17)	8.08 (0.06)	3.4 (0.10)	18.3 (0.69)	1.7 (0.14)	0.35 (0.03)	2.77 (0.08)	2.16 (0.07)	2.86 (0.12)	42.5	99.3
A369	18.0 (1.33)	3.11 (0.80)	3.1 (1.34)	23.1 (3.89)	0.8 (0.50)	0.27 (0.36)	0.43 (0.11)	0.35 (0.07)	0.41 (0.13)	40.3	89.9

n.m., not measured.

Analyses are reported in wt%. Errors in parentheses are $\pm 1\sigma$.

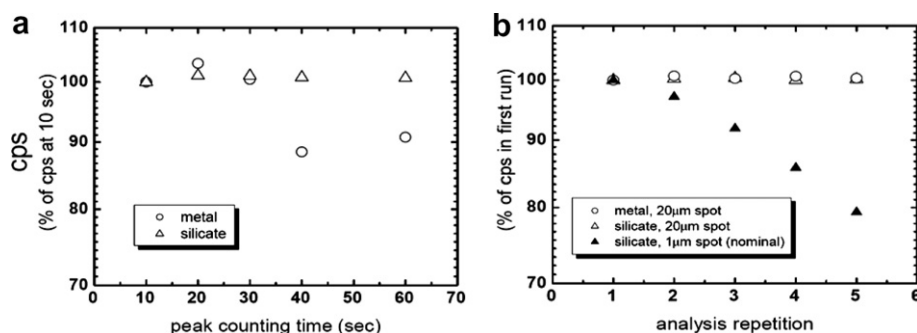


Fig. 3. Variation in counts per second for (a) different counting times and (b) repeated analyses. Analyses in (a) were conducted on separate points, and those in (b) were conducted without changing position. Because Cs was not mobilized by continuous heating on a single spot (b, circles), the deviation from nominal cps in (a) can be attributed to sample heterogeneity. Significant Cs loss was only observed in the silicate phase when using the smallest possible beam (dark triangles).

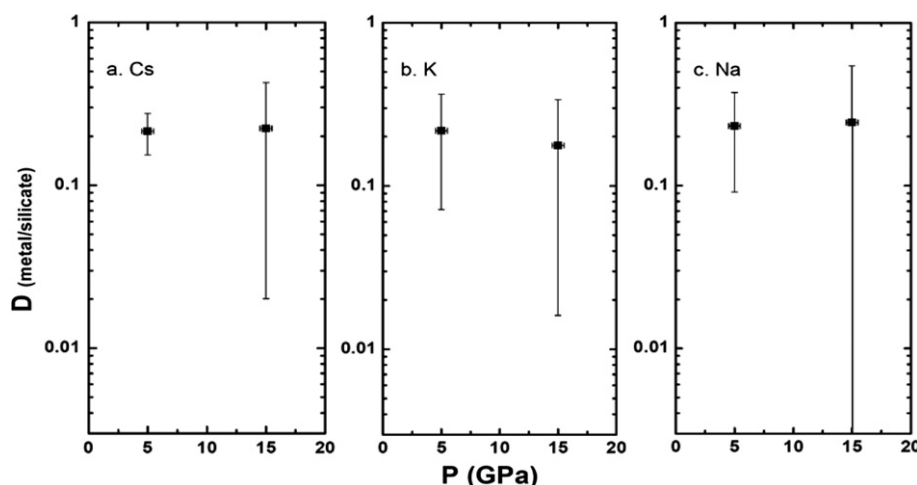


Fig. 4. Variation in metal-silicate partition coefficients with pressure for (a) Cs, (b) K, and (c) Na. Errors are much larger for the 15 GPa run due to the difficulty of dry-polishing the diamond capsule.

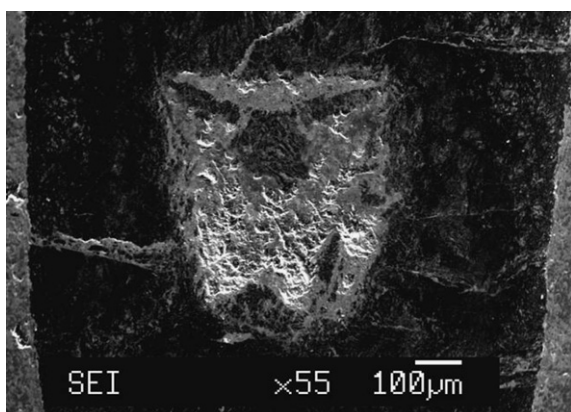


Fig. 5. Secondary electron image of run #A369, which was conducted at 15 GPa. The sample (center) is flat at the top but has a large piece of diamond capsule embedded. It has also been filled in by a contaminant during polishing, most likely pieces of the diamond grinding pad. The bottom of the sample was extremely rough and made identification of individual phases difficult.

unreliable, and are reported without error bars. The D_K in Fig. 8b for the pure Fe composition is approximately 10^{-4} and is not plotted. For compositions above 25 wt% S in the metal, the correlations of D -values for all elements with rising S content are very strong. Similar to the elemental trend in nbo/t , the sensitivity of an element's partitioning behavior appears to be more pronounced for the larger elements.

3.6. Oxygen fugacity

The addition of iron silicide to the starting composition reduced the oxygen fugacity of the run product by approximately two log units. The reduction in overall oxygen fugacity was accomplished by the consumption of oxygen by the reaction $Si + O_2 \rightarrow SiO_2$, where the oxygen was obtained largely at the expense of FeO in the silicate. To maintain the S inventory in the metal phase, elemental S was also added to the starting composition. Some of that S was not dissolved into the metal phase, and the concentration of S in the silicate phase reached as high as 6 wt% (see

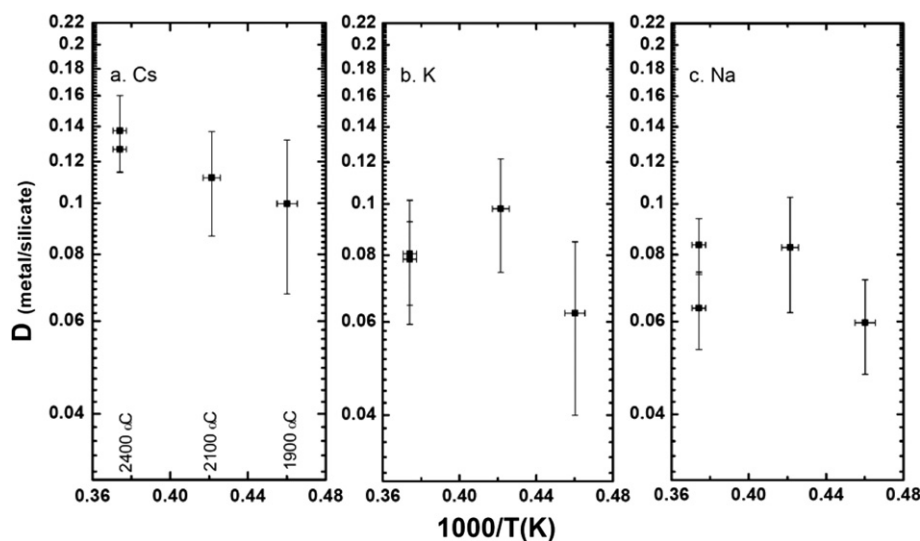


Fig. 6. Variation in metal-silicate partition coefficient with temperature for (a) Cs, (b) K, and (c) Na. High temperature tended to raise the partition coefficient for Cs, but all analyses were within error of each other. Trends are not significant for K and Na, but all D -values reported for K and Na were lower than those for Cs.

Table 3). Similar high S contents in silicate liquid have also been documented by McCoy et al. (1999) in experiments with low fO_2 . Furthermore, the metallic S concentration was somewhat variable in the metal phase, and because S content strongly affects alkali partitioning (see Section 3.5), Fig. 9 displays D -values for each element relative to metallic S content for both reduction conditions.

As with the S-varying experiments, the reduction in S content below 25 wt% yielded D -values that were typically unreliable. Those D -values from analyses below detection limits are displayed without error bars. In the experiments yielding reliable analyses, D_{Cs} and D_K were somewhat high-

er at fO_2 of approximately $\Delta IW = -4.0$ than for the less reduced case of $\Delta IW = -2.0$, but the difference in D -values was usually less than half of an order of magnitude. This result is more significant with the understanding that the addition of SiO_2 from the oxidation of metallic Si tended to reduce the nbo/t of the silicate melt. As we discovered, lowering nbo/t depresses D -values (Fig. 7), so the fact that D_{Cs} and D_K were higher in the reduced, low nbo/t case lends weight to the effect of reduction on Cs and K partitioning. The effect of varying nbo/t is parameterized in Section 4.1 and applied to the oxygen fugacity data, with the resulting D -values displayed in Fig. 14.

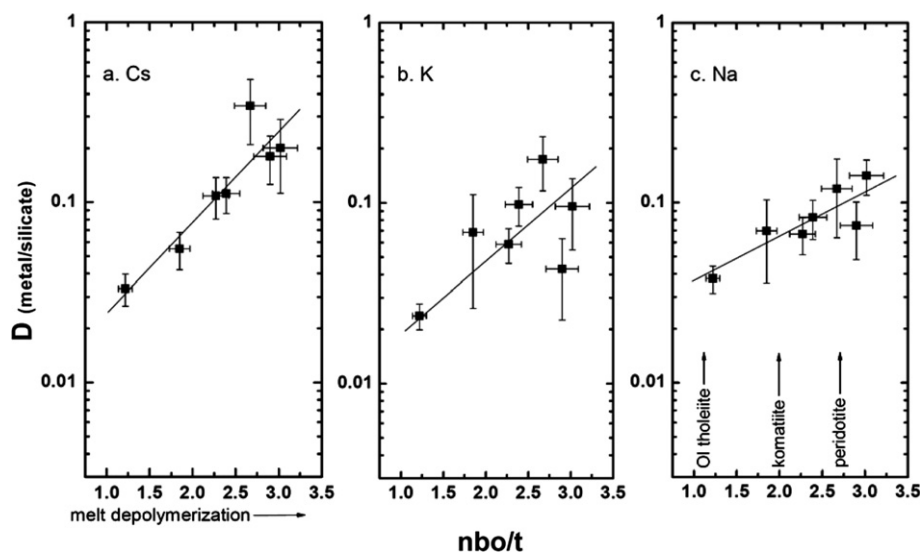


Fig. 7. Variation in metal-silicate partition coefficient with melt polymerization for (a) Cs, (b) K, and (c) Na. D -values for the alkalis rose with rising nbo/t in a fairly regular manner. The correlation of Cs measurements was significantly better than for the other alkalis, even though all were doped to the same starting concentration. It appears that Cs partitioning is the most sensitive to changes in melt polymerization, and that the degree of sensitivity is related to the size of the alkali elements. All experiments of this series were above detection limits.

4. DISCUSSION

4.1. Parameterization of variables

The correlation of D -values with nbo/t (Fig. 7) is complicated by the effect of small variations in metallic S content between the individual runs. As we have shown, very small changes in S yield dramatic differences in partition coefficients (Fig. 8); however, the run products from S-varying experiments also had slightly different nbo/t , so a careful deconvolution of these two variables was warranted. This was accomplished by first conducting a linear regres-

sion of the nbo/t data, and applying the slope of that trend to normalize the S-varying measurements to the same nbo/t . We then regressed the S data, and applied that slope to normalize all the nbo/t -related D -values to the same S content. Normalization of nbo/t data changed the regression slope, which then had to be reapplied to the S data. This iterative process continued until the regression coefficients stabilized. We consider this method of separating the effects of the two parameters to be robust because the regression coefficients stabilized to the same value whether they started too high or too low. All data from the results in Section 3 have been normalized using these regressions,

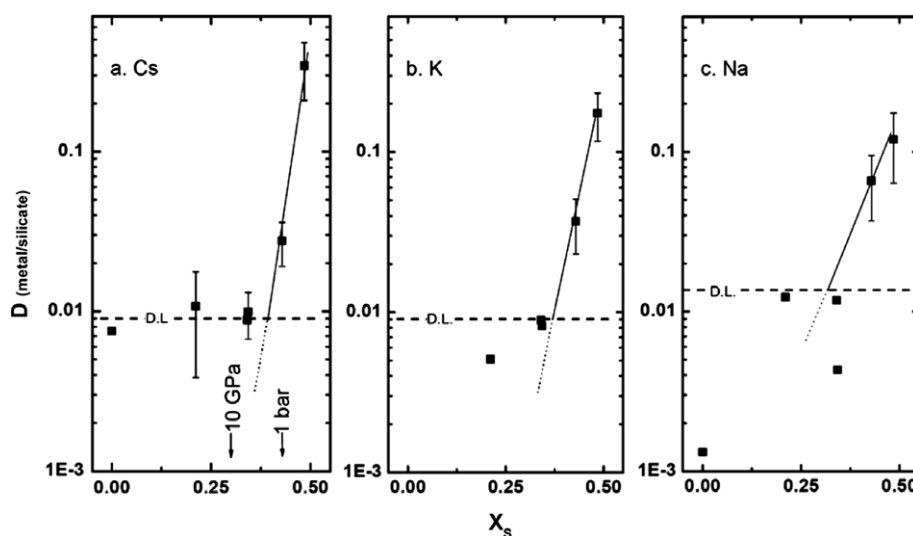


Fig. 8. Variation in metal-silicate partition coefficient with S content for (a) Cs, (b) K, and (c) Na. The majority of experiments below about 25 wt% S in the metal phase yielded analyses that were below detection limits for each element. Above 25 wt%, D -values rise markedly, with the larger alkali elements tending to be more sensitive than the smaller ones. Error bars are $\pm 1\sigma$, and error bars from analyses below detection limits are not shown. The Fe-FeS eutectic composition (Fei et al., 1997) is indicated at 1 bar and 10 GPa.

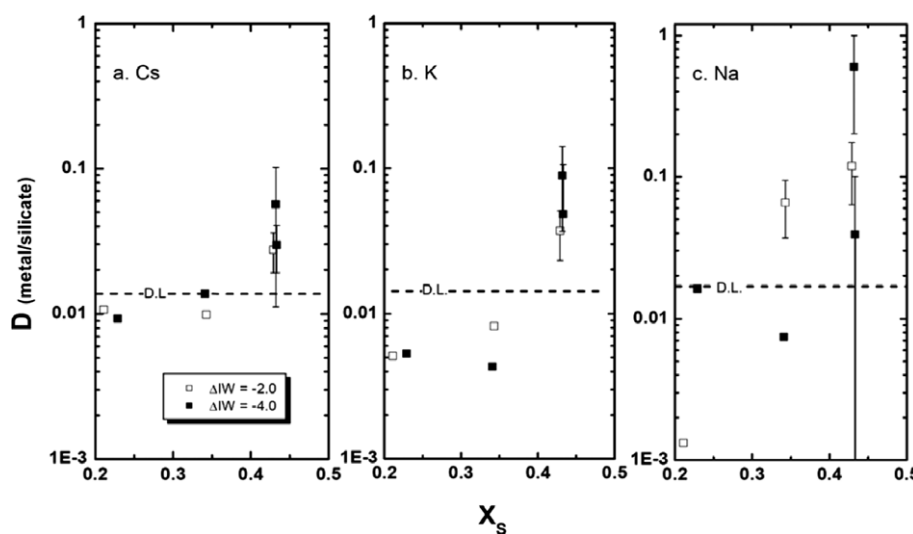


Fig. 9. Variation in metal-silicate partition coefficient with changing oxygen fugacity for (a) Cs, (b) K, and (c) Na. D -values are plotted against final metallic S content for comparison between oxidized and reduced conditions. The redox reaction between FeO and Si drove Si and S into the silicate, lowering both the final S content in the metal and the nbo/t of the silicate melt. Though nbo/t was generally lower for the IW-4.0 condition, D -values were slightly higher for most elements.

and the adjusted figures are presented in Figs. 10–14. We have adopted the notation D^* for the parameterized partition coefficient. For each variable in the sections below, the data were normalized to an nbo/t or X_S value close to the average of all data within that set to avoid distortion introduced by regression to much different conditions. Note that the numerical values used to generate these figures are not reported because they were never actually observed during our analyses and are a product of our numerical regression.

4.1.1. Pressure

Normalization of the pressure-varying data to X_S of 0.45 and nbo/t of 2.6 reveals an apparent negative pressure effect (Fig. 10). This negative trend may be an artifact of the nor-

malization process, since the values of nbo/t were so much different between the two charges. Normalization across nearly the entire range of nbo/t is less reliable than for small differences; nevertheless, we conclude that there is a weak negative pressure effect between 5 and 15 GPa for all the alkalis studied here.

4.1.2. Temperature

The temperature-varying experiments were normalized to X_S of 0.475 and nbo/t of 2.5, with the results displayed in Fig. 11. The weak positive temperature effect suspected in Section 3.3 is magnified after normalization, and is visible for all the alkali elements. The partition coefficients are not as sensitive to temperature as they are to nbo/t or S

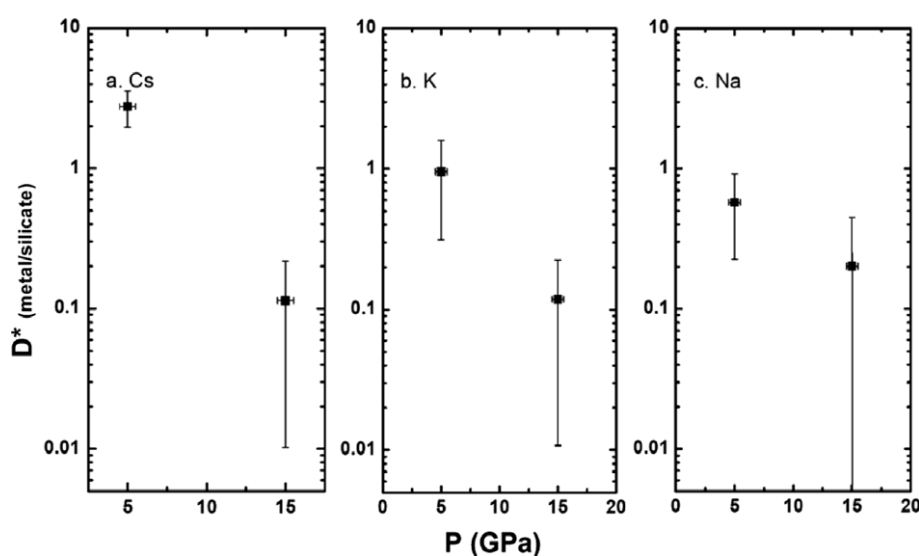


Fig. 10. Variation in metal-silicate partition coefficient with pressure for (a) Cs, (b) K, and (c) Na, with all data normalized to X_S of 0.45 and nbo/t of 2.6. The apparent negative trend with pressure may be an artifact of the normalization process, since the nbo/t values were significantly different between the two charges.

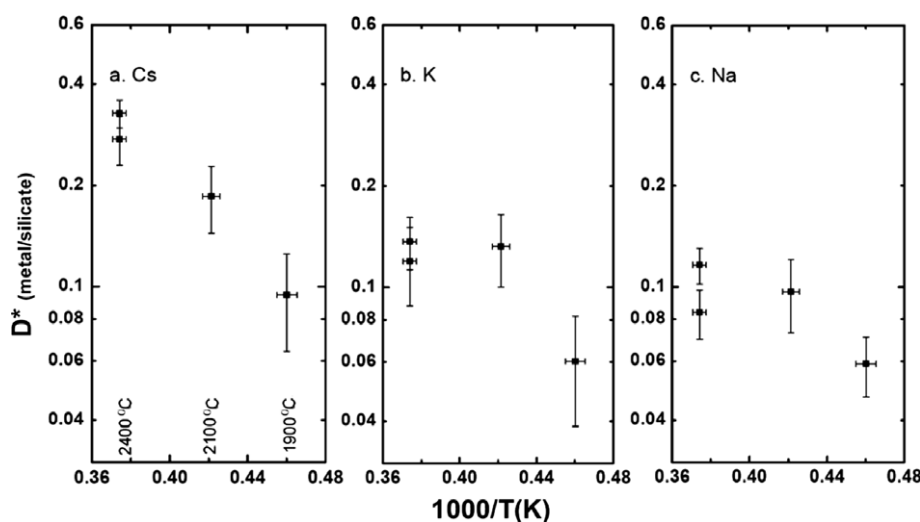


Fig. 11. Variation in metal-silicate partition coefficient with temperature for (a) Cs, (b) K, and (c) Na, with all data normalized to X_S of 0.475 and nbo/t of 2.5. Normalization magnifies the weak positive temperature effect on D -values.

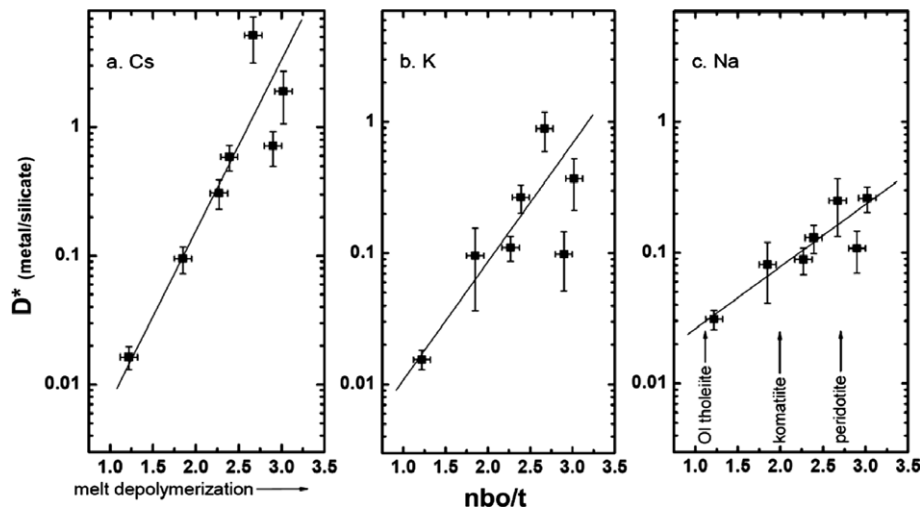


Fig. 12. Variation in metal-silicate partition coefficient with melt polymerization for (a) Cs, (b) K, and (c) Na, with all data normalized to X_S of 0.5. The major difference between this figure and Fig. 7 is the larger scale on the y-axis. The difference in the slope of trendlines is also magnified.

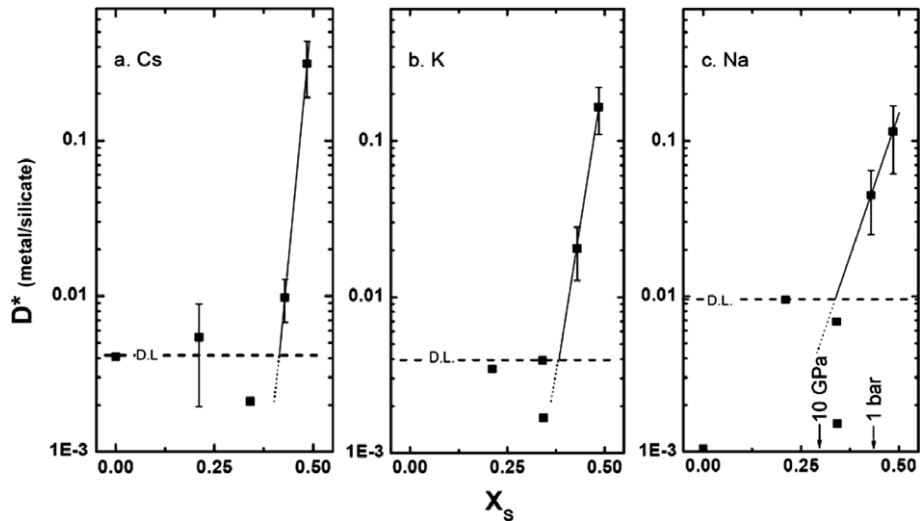


Fig. 13. Variation in metal-silicate partition coefficient with metallic S content for (a) Cs, (b) K, and (c) Na, with all data normalized to nbo/t of 2.7. Normalization yielded a slightly higher slope of the trendline, and retained the positions of individual data points relative to each other.

content, but do change by up to a factor of three across the temperature range we investigated. The range in D -values was greatest for Cs, and least for Na.

4.1.3. Silicate composition

Normalization of data from nbo/t -varying experiments to X_S of 0.5 did not change the relative positions of data points in Fig. 12. The main difference between Fig. 12 and the uncorrected data in Fig. 7 is the scale on the y-axis and the slope of the trendline. The regressions yield the following expressions for D -values as a function of melt polymerization at $X_S = 0.5$:

$$\log D_{Cs} = -3.2 + 1.17 \times (nbo/t)$$

$$\log D_K = -2.4 + 0.67 \times (nbo/t)$$

$$\log D_{Na} = -2.0 + 0.44 \times (nbo/t)$$

4.1.4. Metallic composition

The data from S-varying experiments were normalized to nbo/t of 2.7, and the results are plotted in Fig. 13. As with the adjustment of silicate composition, the results are quite similar to the uncorrected data (Fig. 8). Because only two of the compositions analyzed were above detection limits, it must be understood that the following regression expressions are subject to significant variation based on small deviations in either point.

$$\log D_{Cs} = -12.1 + 23.3 \times X_S$$

$$\log D_K = -7.7 + 13.9 \times X_S$$

$$\log D_{Na} = -4.1 + 6.4 \times X_S$$

4.1.5. Oxygen fugacity

The ambiguity of the effect of oxygen fugacity on alkali partitioning is resolved upon normalization of nbo/t to 2.7.

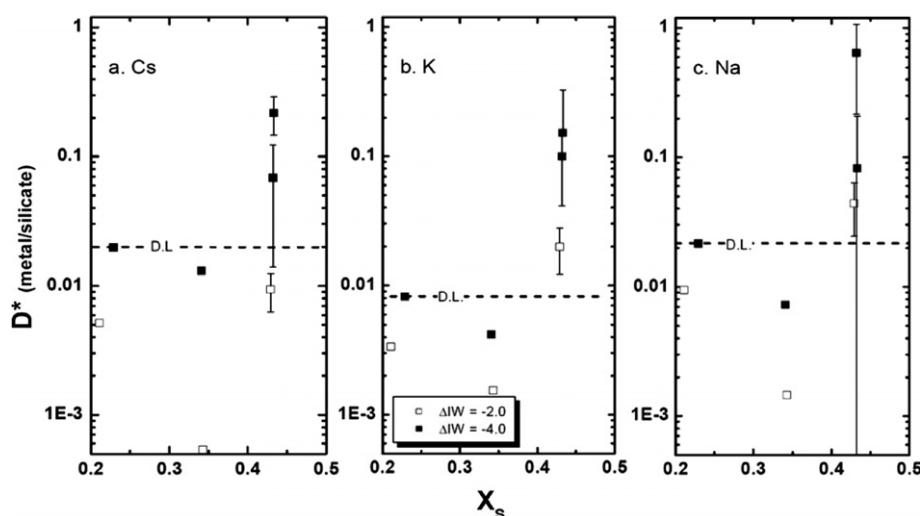


Fig. 14. Variation in metal-silicate partition coefficient with oxygen fugacity for (a) Cs, (b) K, and (c) Na, with all data normalized to nbo/t of 2.7. Deconvolution of the effects of nbo/t in these experiments readily reveals the effect of lowering oxygen fugacity.

In all cases, the more reduced charge had a higher partition coefficient for each element than the less reduced run product. In general, a reduction in oxygen fugacity by two log units yielded a rise in D -value by an order of magnitude. The data imply that for a rise in oxygen fugacity above $\Delta IW = -2.0$, the D -values would be even lower than those shown in Fig. 14.

4.2. Partitioning behavior

The most well-defined trend in the partitioning of Cs is the clear dependence on silicate melt composition. As the melt becomes depolymerized, it appears that Cs becomes less compatible in the silicate phase. One possible explanation for this trend with respect to nbo/t relates to the structure of the silicate melt. In general, the structure of molten silicate is that of a linked network of SiO_4 tetrahedra interrupted by the presence of monovalent or divalent cations, which create non-bridging oxygens (Mysen, 1983). Silicate melts with a high nbo/t are less rigidly structured than are those with low nbo/t , thus are more tightly packed and less likely to incorporate large cations like Cs (Watson, 1976). Therefore, if there are available sites elsewhere (i.e., in the metallic liquid), Cs is more likely to be ejected from a high nbo/t silicate melt than from one with low nbo/t .

The other obvious prerequisite to partitioning of Cs into metal is the presence of about 25 wt% S in the metal phase. The central question regarding this effect concerns what makes the alkali elements chalcophile. Although the explanation for this effect is not as straightforward as that of the nbo/t effect, the analogous question relates to the behavior of siderophile elements, which are more siderophile at low oxygen fugacity. (e.g., Righter, 2003) As with other chalcophile elements, it is clear in this case that sulfur fugacity is the driving force behind an alkali's affinity for the metal phase.

4.3. Comparison of Cs, K, and Na

For a given change in nbo/t , the range in D_{Cs} is more pronounced than for D_K , and the change in D_K is greater than for D_{Na} (Fig. 7). Though this effect is most visible in the change in D -value with nbo/t , it can also be identified in the S-varying experiments (Fig. 8). It appears that the sensitivity of a partition coefficient to changes in run conditions is positively correlated with cation size. Although it is important to remember that the error bars displayed in Figs. 7 and 8 represent only one standard deviation, and care must be taken to avoid over interpreting the results, this apparent dependence on atomic number may be related to the structure and chemistry of the silicate melt.

As outlined in Section 4.2, high nbo/t silicate liquids are more tightly packed, and there is a smaller population of sites available for large cations (Cs) than for small ones (K, Na). Because we infer that one of the driving factors in Cs partitioning is that its large size causes its displacement from the silicate liquid, it follows that cations of a smaller size would have a weaker response. Additionally, high nbo/t melts tend to favor cations that form strong bonds with oxygen (Watson, 1976). Cs, having the lowest charge/radius ratio, will tend to form the weakest bonds. The combination of these two effects renders cations with small ionic radii more compatible in silicate melts with high nbo/t ; therefore, the partition coefficients of K and Na exhibit less drastic changes with varying nbo/t than for Cs.

4.4. Comparison to other work

There have been relatively few metal-silicate partitioning studies for the alkalis (e.g., Chabot and Drake, 1999; Gessmann and Wood, 2002; Murthy et al., 2003), and the ones that have been conducted have not yielded consistent D_K values. This inconsistency is largely due to different compositions, particularly due to small changes in S content. Using our parameterization, described in Section 4.1, we

have normalized the data presented Chabot and Drake (1999), Gessmann and Wood (2002), and Murthy et al. (2003) to $X_S = 0.5$. The change in nbo/t for these three studies is displayed with ours in Fig. 15. After normalization, it is clear that three of these studies have found a similar trend with nbo/t , while Murthy et al. (2003) found the opposite effect on D_K with respect to changing nbo/t . The reason for this discrepancy is not known; however, our trend for nbo/t may be described as $\log D_K = -2.4 + 0.67 \times (nbo/t)$, which is very similar to the regression presented by Chabot and Drake (1999) of $\log D_K = -3.5 + 0.46 \times (nbo/t)$.

In summary, there are some common features in the trends of most studies. For example, this study supports Murthy et al. (2003) in the assertion that the pressure effect for alkali partitioning is very weak. In all studies in which S content was a parameter, partitioning of the alkali elements K and Na rose dramatically with the S content of the metal phase (Chabot and Drake, 1999; Gessmann and Wood, 2002). In all cases, K and Na are completely lithophile in S-free charges.

4.5. Cs and core formation

In order to determine whether Cs is a useful element in constraining core formation conditions, it is necessary to know the D_{Cs} that would explain the observed mantle abundances. Without samples of the core, we must infer what the concentration in the metal phase should be. Our approach was to use the expected abundance from the volatility trend (Fig. 1) as the basis for pre-segregation concentration. We assume that the entire depletion of Cs relative to the volatility trend is due to core extraction; i.e., all of the missing Cs is in the core. Under these assumptions, we calculate the D -value required to generate estimated primitive mantle abundances as follows:

$$D = \frac{C^{\text{metal}}}{C^{\text{silicate}}} = \frac{(C^{\text{expected}} - C^{\text{mantle}}) * \frac{m^{\text{mantle}}}{m^{\text{core}}}}{C^{\text{mantle}}}$$

where C^{expected} is given by the volatility trend, C^{mantle} is measured or estimated from basalts and mantle xenoliths, and m is the mass of subscripted reservoir. An additional uncertainty is introduced due to the difficulty of estimating primitive mantle concentrations (e.g., Kargel and Lewis,

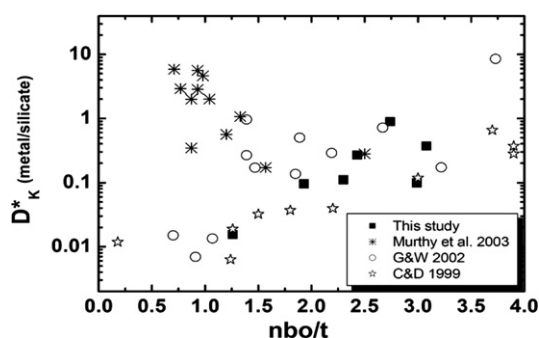


Fig. 15. D_K vs. nbo/t , with data from Chabot and Drake (1999) (stars), Gessmann and Wood (2002) (circles), Murthy et al. (2003) (asterisks) and this study (solid squares). All data have been normalized to $X_S = 0.5$.

1993) due to extensive processing of the upper mantle. This is especially true for lithophile trace elements. Based on various estimates of mantle composition (Lodders, 1995; McDonough, 2004) and the estimated condensation temperature of Cs, the D_{Cs} required to explain its primitive mantle abundance is between 3 and 80.

The maximum D_{Cs} obtained in this study was 0.345. Most conditions required to obtain this D -value were relatively reasonable: nbo/t was 2.7, approximately equal to that of peridotite, and oxygen fugacity was IW-2.0, which is usually assumed to be reasonable for core formation conditions (e.g., Chabot and Drake, 1999; Chabot and Agee, 2003). However, the starting metal composition was pure FeS, which resulted in 33 wt% S in the metal. This is well outside the range of possibilities based on cosmochemical and geophysical arguments, which hold that Earth's core contains no more than 14 wt% S (Brown et al., 1984), and probably less than 5 wt% (Kargel and Lewis, 1993). The precipitous drop in D_{Cs} with decreasing metallic S content, combined with the fact that no other parameter studied here could reasonably raise D_{Cs} by another order of magnitude, precludes the possibility that Cs has been sequestered to Earth's core by simple metal-silicate partitioning. However, based on our results it is certainly possible that a planet with a larger inventory of S and other volatile elements, such as Mars, may incorporate significant amounts of alkali metals into its core.

4.6. Remaining work

Recent work on the solubility of K in Fe has focused on the electronic configuration and associated physical structure transitions of elemental K at pressures above 26 GPa (Lee et al., 2004). This shift, which involves the single valence electron migrating from an s orbital to a d orbital, was predicted by Bukowinski (1976) and demonstrated at room temperature by Takemura and Syassen (1983). At pressures above those that produce the transition, alkali metals may behave more like transition metals, which also have electrons in d orbitals, and display a drastically increased solubility in iron. The $s \rightarrow d$ transition is also applicable to the other alkali elements, with the pressure of that transition lowering for increasing atomic number (Winzenick et al., 1994). The appearance of this effect at 26 GPa for K suggests that the same transition for Cs should be well within the reach of a diamond-anvil cell (DAC) apparatus.

Lee et al. (2004) acknowledged that this phenomenon could allow incorporation of a greater amount of K in the core than is allowed by cosmochemical abundance, and an order of magnitude more than is required to sustain the geodynamo. They also stated that if core segregation was largely complete by the time the earth was large enough to have a magma ocean extending to 26 GPa, that would explain the relatively minor depletion of K in Earth's mantle. By extension to Cs, a lower $s \rightarrow d$ transition pressure would have allowed more Cs to be extracted from the mantle, and would explain the relatively large depletion in the mantle. A similar Cs-bearing DAC experiment could thus be quite revealing.

In addition, a simple metal-silicate partitioning experiment should also be conducted at pressures above the

s → d transition. For K, this work has begun with the experiments of Hirao et al. (2006), and should also be extended to Cs to determine whether the high-pressure partitioning of Cs is radically different than at modest pressures. If so, Cs could still provide a valuable clue to the conditions under which the core segregated.

5. CONCLUSION

We provide the first data set on the partitioning behavior of Cs under varying conditions of pressure, temperature, metal and silicate composition, and oxygen fugacity. Over a temperature range of 1900–2400 °C, there was a weak correlation of D_{Cs} with rising temperature, but the trend was nearly lost in the noise, and was not apparent at all for D_K and D_{Na} . The pressure effect was weakly negative up to 15 GPa, the highest pressure attained in this study. Oxygen fugacity was varied from approximately two log units below the iron–wüstite buffer (IW-2) to IW-4. Normalization these data to nbo/t of 2.7 revealed that the reduction in oxygen fugacity resulted in a rise in D -values for all alkalis by approximately an order of magnitude. As reported in other experiments (e.g., Chabot and Drake, 1999; Gessmann and Wood, 2002), D_{Na} and D_K were strongly correlated with nbo/t, and this correlation held for D_{Cs} as well. The strongest dependence for all the alkalis in this study was on S content of the metal phase, with S contents above 25% strongly raising D -values. Overall, the relative effects of each parameter are broadly consistent with other alkali partitioning studies, but in most cases the absolute D -values measured are much different, even for K and Na under almost identical conditions.

Although clear trends are evident for some of these parameters, they are not pronounced enough to raise cesium's metal-silicate partition coefficient high enough to explain its depletion in Earth's mantle without resorting to unreasonable core formation conditions. It is possible that future work concentrating on the high-pressure electronic transition of Cs will discover partition coefficients much higher than those measured in this study of moderate-pressure partitioning.

ACKNOWLEDGMENTS

We thank V. Murthy, R. Dwarzski, and W. McDonough, A. Brandon, and two anonymous reviewers for their thoughtful suggestions and comments that improved the quality of this manuscript. We also thank M. Spilde, for assistance with the electron microprobe. This work was supported by C. Agee's NASA Cosmochemistry grant.

REFERENCES

- Agee C. B., Li J., Shannon M. C. and Circone S. (1995) Pressure–temperature phase diagram for the Allende meteorite. *J. Geophys. Res.* **100**, 17725–17740.
- Bouhifd M. A. and Jephcoat A. P. (2003) The effect of pressure on partitioning of Ni and Co between silicate and iron-rich metal liquids: a diamond-anvil cell study. *Earth Planet. Sci. Lett.* **209**, 245–255.
- Brown J. M., Ahrens T. J. and Shampine D. L. (1984) Hugoniot data for pyrrhotite and the Earth's core. *J. Geophys. Res.* **89**, 6041–6048.
- Bukowinski M. S. T. (1976) The effect of pressure on the physics and chemistry of potassium. *Geophys. Res. Lett.* **3**, 491–494.
- Chabot N. L. and Agee C. B. (2003) Core formation in the earth and moon: new experimental constraints from V, Cr, and Mn. *Geochimica et Cosmochimica Acta* **67**, 2077–2091.
- Chabot N. L. and Drake M. J. (1999) Potassium solubility in metal: the effects of composition at 15 kbar and 1900 °C on partitioning between iron alloys and silicate melts. *Earth Planet. Sci. Lett.* **172**, 323–335.
- Chabot N. L., Draper D. S. and Agee C. B. (2005) Conditions of core formation in the earth: constraints from nickel and cobalt partitioning. *Geochimica et Cosmochimica Acta* **69**, 2141–2151.
- Fei Y., Bertka C. M. and Finger L. W. (1997) High-pressure iron–sulfur compound, Fe_3S_2 , and melting relations in the Fe–FeS system. *Science* **275**, 1621–1623.
- Gessmann C. K. and Rubie D. C. (1998) The effect of temperature on the partitioning of nickel, cobalt, manganese, chromium, and vanadium at 9 GPa and constraints on formation of the Earth's core. *Geochimica et Cosmochimica Acta* **62**, 867–882.
- Gessmann C. K. and Wood B. J. (2002) Potassium in the Earth's Core? *Earth Planet. Sci. Lett.* **200**, 63–78.
- Hirao N., Ohtani E., Kondo T., Endo N., Kuba T., Suzuki T. and Kikegawa T. (2006) Partitioning of potassium between iron and silicate at the core-mantle boundary. *Geophys. Res. Lett.* **33**, L08303.
- Jaeger W. L. and Drake M. J. (2000) Metal–silicate partitioning of Co, Ga, and W: dependence on silicate melt composition. *Geochimica et Cosmochimica Acta* **64**, 3887–3895.
- Jones J. H. and Walker D. (1991) Partitioning of siderophile elements in the Fe–Ni–S system: 1 bar to 80 Kbar. *Earth Planet. Sci. Lett.* **105**, 127–133.
- Kargel J. S. and Lewis J. S. (1993) The composition and early evolution of the Earth. *Icarus* **105**, 1–25.
- Lee K. K. M., Steinle-Neumann G. and Jeanloz R. (2004) Ab-initio high-pressure alloying of iron and potassium: implications for the Earth's core. *Geophys. Res. Lett.* **31**, GL019839.
- Li J. and Agee C. B. (1996) Geochemistry of mantle-core differentiation at high pressure. *Nature* **391**, 686–689.
- Lodders K. (1995) Alkali elements in the Earth's core: evidence from enstatite meteorites. *Meteoritics* **30**, 93–101.
- McCoy T. J., Dickinson T. L. and Lofgren G. E. (1999) Partial melting of the Indarch (EH4) meteorite: a textural, chemical and phase relations view of melting and melt migration. *Meteoritics Planet. Sci.* **34**, 735–746.
- McDonough W. F. (2004) Compositional model for the Earth's core. In *Treatise on Geochemistry*, vol. 9 (eds. H. D. Holland and K. K. Turekian). Elsevier Pergamon, San Diego, pp. 547–568.
- McDonough W. F. and Sun S.-S. (1995) The composition of the Earth. *Chem. Geol.* **120**, 223–254.
- Murthy R. M., van Westrenen W. and Fei Y. (2003) Experimental evidence that potassium is a substantial radioactive heat source in planetary cores. *Nature* **423**, 163–165.
- Mysen B. O. (1983) The structure of silicate melts. *Ann. Rev. Earth Planet. Sci.* **11**, 75–97.
- Mysen B. O. and Virgo D. (1980) Trace element partitioning and melt structure: an experimental study at 1 atm pressure. *Geochimica et Cosmochimica Acta* **44**, 1917–1930.
- Palme H. and O'Neill H. St. C. (2004) Cosmochemical estimates of mantle composition. In *Treatise on Geochemistry*, vol. 2 (eds. H. D. Holland and K. K. Turekian). Elsevier Pergamon, San Diego, pp. 1–38.

- Richter K. (2003) Metal-silicate partitioning of siderophile elements and core formation in the early earth. *Ann. Rev. Earth Planet. Sci.* **31**, 135–174.
- Richter K. and Drake M. J. (2000) Metal/silicate equilibrium in the early earth – new constraints from the volatile moderately siderophile elements Ga, Cu, P, and Sn. *Geochimica et Cosmochemica Acta* **64**, 3581–3597.
- Richter K., Drake M. J. and Yaxley G. (1997) Prediction of siderophile element metal-silicate partition coefficients to 20 GPa and 2800 °C: the effects of pressure, temperature, oxygen fugacity, and silicate and metallic melt compositions. *Phys. Earth Planet. Int.* **100**, 115–134.
- Takemura K. and Syassen K. (1983) High-pressure phase transitions in potassium and phase relations among heavy alkali metals. *Phys. Rev. B* **28**, 1193–1196.
- Wade J. and Wood B. J. (2005) Core formation and the oxidation state of the earth. *Earth Planet. Sci. Lett.* **236**(1–2), 78–95.
- Wänke H. (1981) Constitution of the terrestrial planets. *Phil. Trans. R. Soc. London Ser. A* **303**, 287–302.
- Watson E. B. (1976) Two-liquid partition coefficients: experimental data and geochemical implications. *Contr. Min. Pet.* **56**, 119–134.
- Winzenick M., Vijayakumar V. and Holzapfel W. B. (1994) High-pressure X-ray diffraction on potassium and rubidium up to 50 GPa. *Phys. Rev. B* **50**, 12381–12385.

Associate editor: Alan D. Brandon